



CMD 23-M27.11

Date: 2023-08-01

File / dossier : 6.02.04

Edocs pdf : 7099918

Oral presentation

Exposé oral

**Written submission from
Paul Sedran, RESD Inc.**

**Mémoire de
Paul Sedran, RESD Inc.**

Bruce Power

Bruce Power

**Bruce Power Mid-Term Update of
Licensed Activities**

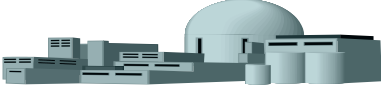
**Rapport de mi-parcours au sujet
des activités autorisées de Bruce
Power**

Commission Meeting

Réunion de la Commission

September 20 and 21, 2023

Le 20 et 21 septembre 2023

 RESD Inc.	Document Identification				
	<small>Project</small>	<small>Type</small>	<small>Division</small>	<small>Serial</small>	<small>Revision</small>
	CNSC 004	REPT	ENG	0001	00
<small>Date Effective:</small>			<small>Retain Until:</small>		
Aug 03, 2023			Aug 03, 2030		

Review of Submissions on Elevated Heq in
 Pressure Tube Rolled Joints for the Midterm
 Review of Bruce Power Licensed Activities

P Sedran

Prepared by: Paul Sedran, P.Eng
 Principal, RESD Inc

Date: August 3rd, 2023

Definition of Abbreviations and Symbols

BM	Burnish Mark
C_D	Concentration of D in Solution in the PT
D	Deuterium
[D]	Bulk Concentration of D
Heq	Hydrogen Equivalent Concentration
PT	Pressure Tube
PT r_m	PT mean radius
RJ	Rolled Joint
y	Circumferential distance = PT $r_m \theta$
θ	Angular position around the PT wrt Top Dead Centre

1. Introduction

Based on Pressure Tube (PT) fracture toughness considerations, the Power Reactor Operating Licence (PROL 18.01/2028) for the Bruce reactors specifies a maximum allowable hydrogen equivalent (Heq) concentration of 120 ppm for the PTs.

In July, 2021, Bruce Power discovered, for the first time, that the Heq concentration in a PT in the Bruce Nuclear Generating Stations had exceeded the 120 ppm limit. In particular, the PT removed from Fuel Channel B6S13 was found to have an Heq measurement of 211 ppm at the burnish mark (BM) and 212 ppm 10 mm inboard the BM. In addition, several PTs in Bruce Unit 3 were found to exceed 120 ppm near the location of the BM.

The discovery of elevated Heq concentrations in Bruce Units 3 and 6 was communicated to the CNSC, who issued Designated Officer Orders to Bruce Power, Ontario Power Generation, and NB Power, on July 26, 2021.

As a result of the Designated Officer Orders, various documents were submitted to the CNSC by Bruce Power.

Under the CNSC's Participant Funding Program for the public hearing of November 3rd, 2022, the Bruce Power submissions to the CNSC were reviewed independently by the author, as reported in Reference [1], with the primary objective of investigating the hypothesis that the elevated Heq concentrations observed at the top of PT B6S13 are attributable to thermal H/D diffusion from the bottom of the PT to an area of reduced temperature at the top of the PT. In [1], a simplified diffusion analysis was performed to see if the deuterium concentration profiles observed in B6S13 were due to thermal diffusion. The conclusion at the time, from the simplified analysis (which had not been subject to QA verification) was that thermal diffusion alone would have not been sufficient to create the observed [D] (D concentration) profiles

Subsequent to the public hearing of November 3rd, 2022, the CNSC is conducting a Mid-Term Review of licensing activities for Bruce Power, the public hearing for which is scheduled for September 2023. As part of the intervention for the upcoming public hearing, the author has reviewed submissions provided by Bruce Power on the topic of H/D diffusion in the RJs of B6S13, presented in References [2] and [3], and under the scope of the review, performed a revised diffusion analysis for the outlet RJ of B6S13, based on comments by Bruce Power at the meeting of November 3rd, 2022.

Summaries of the review and the revised diffusion analysis are provided in this report.

The revised diffusion analysis comprises Sections 2 – 7 and Appendix 1 of this report.

The reviews of References [2] and [3] are found in Appendix 2.

2. Technical Background

2.1 Diffusion Mechanisms for H/D in the PT RJ

The rupture of PT P2G16 in August 1983 provided a drastic example of the propensity for zirconium to absorb hydrogen (H) and deuterium (D) and for H/D to diffuse within the PT, in this case with severe consequences for PT integrity. Since then, the industry has conducted research and extensive material surveillance programs that have resulted in the development of predictive models for the ingress and redistribution of H/D in PTs, one for the distribution of H/D in the body of the PT, and a separate model for the distribution in the PT Rolled Joint (RJ).

The general equation for the diffusion of H/D in the RJ of the PT is given below.

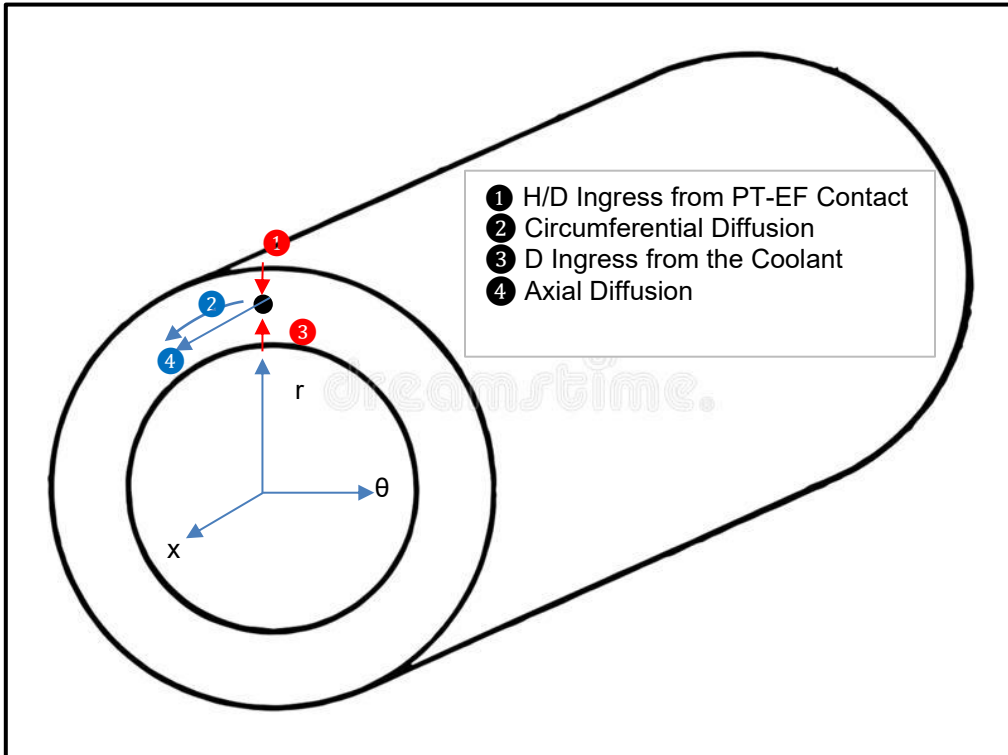
$$\text{grad}(C(x,y,z,t)) = D \nabla^2 C(x,y,z,t) + S(x,y,z,t)$$

The diffusion of H/D into the PT RJ and redistribution of H/D is determined by 2 ingress mechanisms (1 and 2, below) and three diffusion mechanisms (3, 4, and 5) :

1. Electrochemical Diffusion of H/D from the EF into the PT RJ based on Raoult's law,
2. Diffusion of D through the PT inside surface oxide, not covered in this assessment,
3. Thermal Diffusion of H/D within the PT RJ based on Sorret's law,
4. Elastodiffusion of H/D within the PT RJ,
5. Concentration gradient driven diffusion of H/D within the PT RJ under Fick's law.

The geometry of ingress/diffusion for the PT RJ is illustrated in Figure 1, below.

Figure 1- Schematic of PT RJ Diffusion



Note that in the diffusion equations, the dimension in the circumferential direction, θ , is represented by y , where

$$y = r_m \theta$$

and r_m is the mean radius of the PT.

For this assessment, no quantitative analysis of through-wall (radial) diffusion and concentration differences has been performed.

The technical background on the above diffusion mechanisms, relevant to the analyses in this assessment, is presented below.

2.2 Diffusion of H/D in a Concentration Gradient based on Fick's law

In the event that local diffusion of H/D causes a local build up of H/D in an area of the PT, a concentration gradient will be established in the PT material. Fick's law states that the concentration gradient would drive the diffusion of H/D down the concentration gradient, i.e. atoms would migrate from the material with a higher concentration to the area with a lower concentration.

For a concentration gradient of $\text{grad}(C)$, the flux in any direction due to Fick's diffusion is given by:

$$\mathbf{J} = -D \nabla (C) \dots\dots\dots 1$$

In the case of circumferential diffusion (in the θ direction) studied here, Equation 3 becomes

$$\mathbf{J} = -D \frac{\partial C}{\partial y} \dots\dots\dots 2$$

2.3 Thermal Diffusion of H/D based on Sorret's law

When in solution inside the PT material, should H/D be exposed to a temperature gradient, $\text{grad}(T)$, the H/D atoms will diffuse down the temperature gradient, as predicted by Sorret's law:

$$\mathbf{J} = \frac{-DQC}{RT^2} \nabla (T) \dots\dots\dots 3$$

In Equation 5, Q is the activation energy for diffusion and T is the absolute temperature.

In the case of circumferential diffusion (in the θ direction) studied here, Equation 5 becomes

$$\mathbf{J} = \frac{-DQC}{RT^2} \frac{\partial T}{\partial y} \dots\dots\dots 4$$

2.4 Temperature Gradient at the Outlet of B6S13

In the Bruce Power submissions, there are references to a cold spot at the outlet end of the PT, at the top of the PT. For the purpose of this assessment, it was assumed that the temperature gradient in question would have been produced by flow by-pass as a result of diametral creep of the PT.

As a result of PT diametral creep, a space will develop between the top of the fuel bundle and the top of the PT with time in-service, centred at bundles 8 – 10, depending on the fuel channel and station. Flow by-pass involves the diversion of about 35% of the flow, at maximum, into the space above the bundle, instead of flowing through the subchannels inside the bundle.

Consequently, with flow by-pass, less heat will be transferred to the flow at the top of the PT compared with the rest of the flow in the PT, leading to lower temperatures at the top of the PT.

Figure 2 presents a predicted coolant temperature in a PT with flow by-pass.

The temperatures presented in Figure 2 were extracted from ASSERT computations of the temperatures of the coolant in the flow subchannels in a crept PT, noting that subchannel 60 is at the top of the PT where flow bypass occurs and subchannel 51 is at the bottom of the PT.

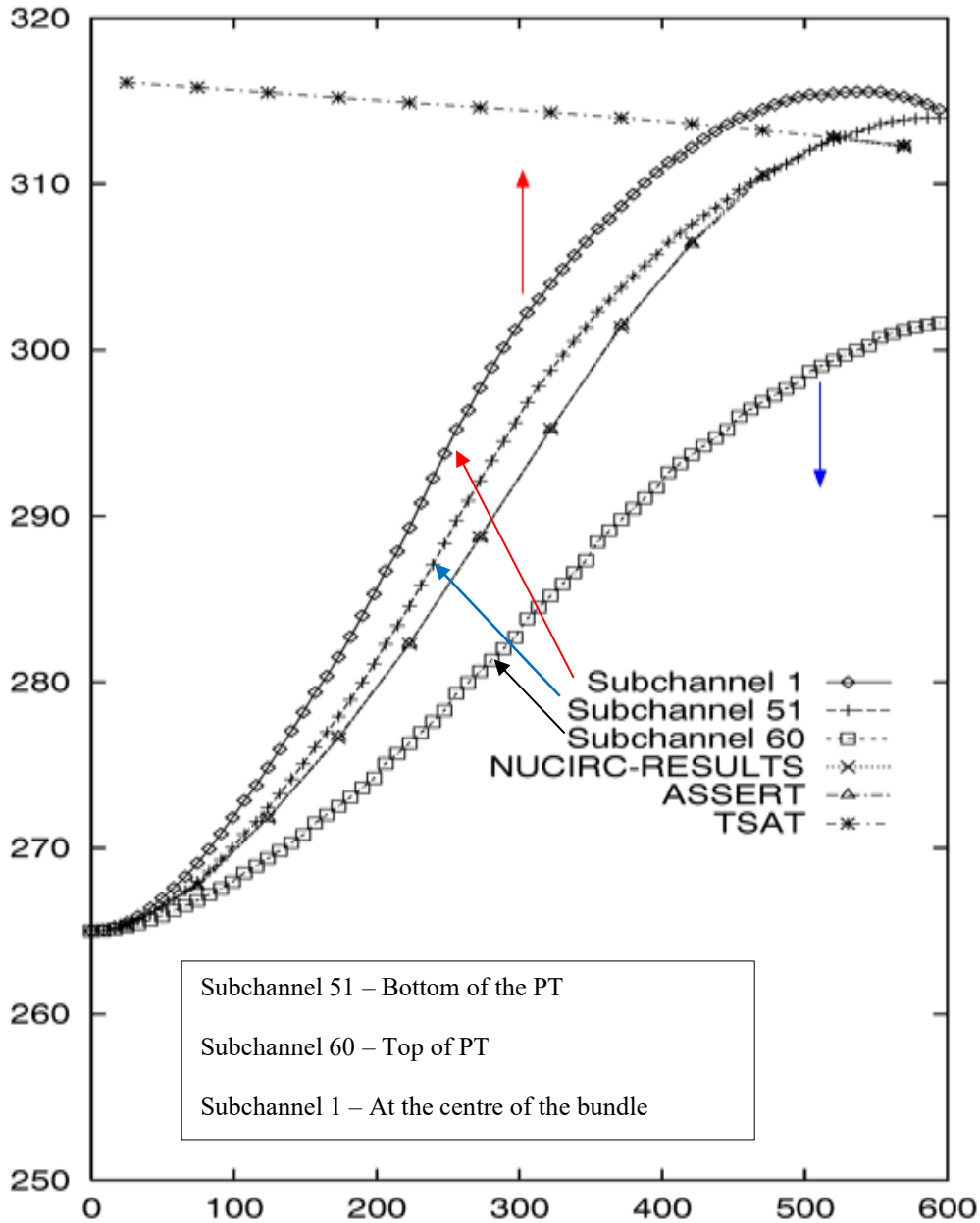
For this assessment it was assumed that the temperature of PT would equal that of the coolant in contact with it and that the temperature at the bottom half of the PT would equal the normal operating temperature at the outlet, which is 308 °C.

As in the previous assessment of Reference [1], it was assumed that operating temperature at the 3 o'clock position ($\theta = 1.571$ rad) at the outlet BM would have been 308 °C for the entire 271279 HH of operation for B6S13. The later assumption is considered reasonable since the flow distributions at the 3, 6, and 9 o'clock positions would not be significantly altered by PT diametral creep. In that case, there would have been a 12 °C difference between the top and side of the PT at the outlet, due to flow bypass, at 271279 HH, based on Figure 2.

For this assessment, based on the above, it was assumed that at 271279 HH, the outlet BM operating temperature was 296 °C at the top of the PT and 308 °C at the side of the PT in B6S13.

The analyses in Section 4 consider the diffusion of D at specific times previous to 271279 HH. For these cases, it was assumed that the side-to-top temperature difference was zero at zero HH and that for intermediate HH values, the temperature difference was linear with HH from 0 to 271279 HH.

Figure 2
Plot of Coolant Temperatures in a PT with Flow Bypass



The figure shows that in a crept PT, the coolant temperature is approximately 12 °C lower at the top of the PT outlet than at bottom of the PT outlet. From the geometry of the fuel bundle and the crept PT, it was assumed that the coolant temperature at both sides of the PT would equal that at the bottom, so that the PT temperature would increase by 12 °C from 0 radians (Top Dead Centre) to $\pi/2$ radians (3 o'clock).

2.6 Bruce Power's Hypothesis for the Cause of Elevated Heq Measurements


The current theory held by Bruce Power is that the elevated [H/D] levels at the top of the PT due to the diffusion of H and D to a cold spot at the top of the PT from an adjacent region of the PT. There are several statements of this hypothesis in the Bruce Power submissions but the most demonstrative was found in CMD 21-H11.2A, which is reproduced as Figure 3, below

Figure 3
Slide 19 of Bruce Power Presentation of September 21, 2021

Understanding the Mechanism

- Higher hydrogen concentrations are encountered in some pressure tubes and are consistently found at top of tube in a narrow region of interest.
 - For affected pressure tubes, measurements in areas outside of the region of interest at top of the tube are significantly lower and within traditional model predictions.
- Hydrogen redistribution is occurring due to a temperature gradient at outlet ends.
 - Analysis has been completed based on recent results to understand this mechanism.

Elevated hydrogen concentrations are limited to a small portion of the pressure tube as determined through extensive scrape sampling and surveillance results.


19

In addition to the thermal diffusion hypothesis, there is a secondary contention that the thermal diffusion is a redistribution process. The implication is that the total amount of H/D in the B6S13 outlet PT RJ is not abnormally high, but could be in the normal range.

The two hypotheses will be denoted as the thermal diffusion theory, and the H/D redistribution theory.

3. B6S13 Outlet BM H/D Concentration Data

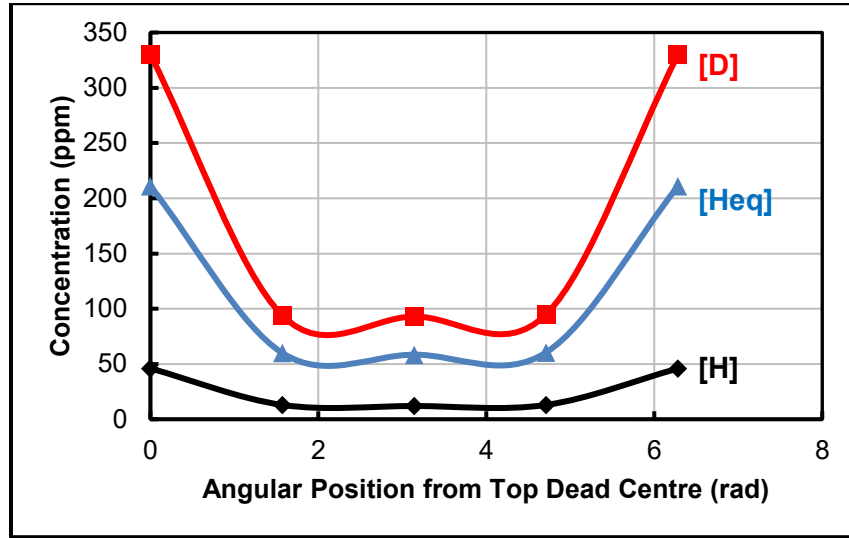
The bulk H and D concentration data used in this assessment are presented in Table 1. The data are based on measurements at the outlet BM, taken from Table A-2 in Attachment A of CMD21-M37-1.

Table 1
H, D, and Heq Concentrations for the Outlet BM

θ		[H]	[D]	Heq
Clock	(rad)	(ppm)	(ppm)	(ppm)
12	0	22	330	187
3	1.571	11.8	94	58.8
6	3.142	12.5	93	59
9	4.712	12.2	95	59.7
12	6.283	22	330	187

The concentration measurements of Table 1 are plotted versus θ in Figure 4.

Figure 4
Circumferential Distribution of [H], [D], and [Heq] at the Outlet
PT BM of B6S13 at 271 729 HH



4. Analysis of the Deuterium Concentration Data for the Outlet BM of B6S13

Section 4.1 presents a condensed summary of the diffusion analysis from [1] for the circumferential diffusion of D from the side to the top of the PT at the outlet RJ BM. A revised diffusion analysis is summarised in Section 4.2.

4.1 Circumferential Deuterium Diffusion Analysis of Reference [1]

As presented in Reference [1], a significant deuterium concentration gradient was measured at the outlet BM in B6S13 at 271279 HH. The bulk deuterium concentration profile is presented in Figure 5. As shown Figure 5, the deuterium in the concentration profile is subject to a thermal diffusive force, driving diffusion up the concentration profile and a Fick's diffusive force driving deuterium down the concentration profile. An analysis of the diffusion for this case was performed to predict the temperature gradient that would have been necessary to generate the deuterium profile in question.

The results of the analysis are presented in Table 2.

Figure 5
Curve Fit to [D] vs θ at the Outlet RJ BM of B6S13 at 271279 HH

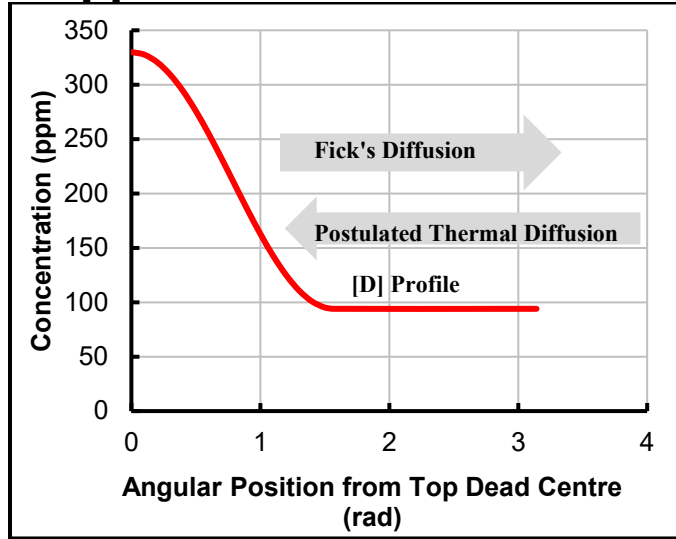


Table 2
Prediction of the Temperature Gradients Required to Generate the H Concentration Gradients of Figure 4

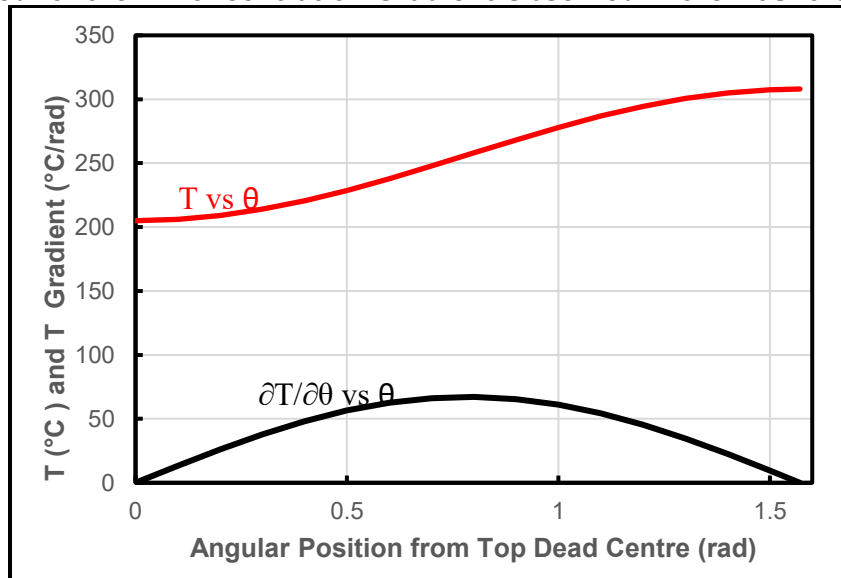
Case	r_m	$\partial c/\partial y$	Q	R	T	T	C	$\partial T/\partial y$	$\partial T/\partial \theta$	$\Delta \theta$	ΔT	$T_{0 \text{ rad}}$
	(m)	(ppm/m)	(J/mol)	($\text{JK}^{-1}\text{mol}^{-1}$)	($^{\circ}\text{C}$)	(K)	(ppm)	($^{\circ}\text{C}/\text{m}$)	($^{\circ}\text{C}/\text{rad}$)	(rad)	($^{\circ}\text{C}$)	($^{\circ}\text{C}$)
1	0.054	358.8	47279	8.313	256.3	529.5	29	609.3	32.928	1.571	51.7	204.6
2	0.054	358.8	33600	8.313	239.7	512.9	29	804.5	43.474	1.571	68.3	171.4

Table 2.1
Nomenclature for Table 2

r_m	Mean Radius of the B6S13 Outlet PT RJ
$\partial c/\partial y$	Concentration gradient
Q	Activation energy for H in Zr
R	Gas constant
T	Absolute temperature at solution point
C	Local concentration at solution point
$\partial T/\partial \theta$	Temperature gradient
$\Delta \theta$	Change in angular position along diffusion path
ΔT	Change in temperature along diffusion path
$T_{0 \text{ rad}}$	Temperature at 0 radians resulting from ΔT

A graphical summary of the entire circumferential temperature profile prediction, presented above, is provided in Figure 6, below.

Figure 6
Predicted Temperature and Temperature Gradient
Required for the D Concentration Gradient Observed in the B6S13 Outlet RJ



The predicted temperature profile of Figure 6 is for Case 1 of Reference [1], giving the highest temperature at the top of the PT, which represents the most favourable result in support of the thermal diffusion theory.

As seen Figure 6, it is predicted that a considerable circumferential temperature gradient would have had to be in existence at the outlet BM of B6F13 to create the circumferential concentration gradients observed. The resulting temperatures at the top of the PT, $T_{0 \text{ rad}}$, appear to be reasonable, in comparison to the channel outlet temperature.

In summary, the assessment of Table 2 indicated that the minimum top-to-side temperature difference required to generate the observed concentration gradients in the B6S13 is 52 °C, compared with an expected temperature difference of 12 °C, from Figure 2.

Based on the above results, thermal diffusion alone could have not caused the observed [D] gradients at the outlet BM of B6S13, noting the simplified method and the lack of QA verification for the analysis. *It should be noted that the analysis of Section 4.1 was revised in Section 4.2 and that the above conclusion has been superseded by this report.*

4.2 Revised Circumferential Diffusion Analysis

The analysis of Reference [1], summarised in Section 4.1, was reviewed by Bruce Power, who commented that the analysis was over-simplified since hydride precipitation and dissolution (ratcheting) had not been accounted for. This was immediately recognized by the author as an important technical feature that had been overlooked in the 1 dimensional diffusion model.

The diffusion analysis of Reference [1] was revised to account for hydride precipitation and dissolution during reactor operation and is summarised in this section. It will be noted that with

hydride ratchetting, the dissolved D gradient will be lower than that in Reference [1], so that the resistance to diffusion up the gradient would be lower.

4.2.1 Prediction of Instantaneous D Flux at 271729 HH

The first step in the analysis was to predict the instantaneous D flux that would have occurred at 271279 HH under the expected thermal gradient due to flow bypass. The calculation would provide a quick test of the Bruce Power hypothesis, which requires that there must have been a D flux from the side of the PT to the top at 271279 HH. Is this was the case, then the hypothesis is supported.

To predict the rate of D diffusion to the top of the PT, the following equation was used

$$J = -D \frac{dC_D}{dy} - \frac{DQC_D}{RT^2} \frac{dT}{dy} \dots\dots\dots 5$$

A summary of the instantaneous flux calculation is provided in Tables 3.1 through 3.3. Table 3.1 presents a summary of the D mass flux calculation and Table 3.1 gives values of the physical constants in the calculation. The symbols in Tables 3.1 and 3.2 are defined in Table 3.3.

Table 3.1
Summary of Instantaneous D Mass Flux Calculation for Diffusion to the Top of the PT at the Outlet RJ BM of B6S13 at 271279 HH

θ	T	C_D	C_D	ΔC_D	$\Delta\theta$	$\Delta C_D/\Delta y$	$J_{\Delta c}$	ΔT	$\Delta T/\Delta y$	$J_{\Delta T}$	J_{total}
(rad)	(°C)	(ppm)	(kg m ⁻³)	(rad)	(kg m ⁻⁴)	(kg m ⁻² s ⁻¹)	(°C)	(°C/m)	(kg m ⁻² s ⁻¹)		
1.571	308	94.0	0.605	-0.170	1.571	-1.998	1.59E-10	-12.0	-141.4	8.15E-11	2.4E-10
0	296	67.7	0.436								

Table 3.2
Physical Constants for the Diffusion Analysis of Table 3.1

PT r_m	Δy	D_D	Q	R	ρ_{PT}
(m)	(m)	(m ² s ⁻¹)	(J/mol)	(JK ⁻¹ mol ⁻¹)	(kg m ⁻³)
0.054	0.085	7.96E-11	33600	8.313	6440

Table 3.3
Definition of Symbols for Tables 3.1 and 3.2

θ	Angular position from Top Dead Centre
T	Temperature
D_H	Diffusion coefficient for H
D_D	Diffusion coefficient for D
C_D	Concentration of D in solution
ρ_{PT}	Density of PT material (including D)
ΔC_D	Difference in C_D
$\Delta\theta$	Difference in θ
PT r_m	Mean radius of the PT
Δy	Difference in the y coordinate
$\Delta C_D/\Delta y$	C_D gradient wrt y
$J_{\Delta c}$	D mass flux due to C_D gradient
Q	
R	Gas constant
ΔT	Temperature difference
$\Delta T/\Delta y$	T gradient wrt y
$J_{\Delta T}$	D mass flux due to T gradient
J_{total}	Total D mass flux due to C_D and T gradients

As seen in the Table 3.1, with the D flux being positive, it is predicted that the thermal gradient would have driven D to the top of the PT at 271279 HH. This result supports the Bruce Power hypothesis but it was recognized that more than the instantaneous rate of diffusion at 271279 HH is required. Addition work, which follows this section, was required to investigate the diffusion of D from 0 to 271279 HH.

4.2.2 Prediction of Time Dependent D Flux from 0 to 271279 HH

The D flux to the top of the PT, presented in Table 3.1 for operation at 271279 h, is an instantaneous value that depends on the temperature and concentration gradients from the side to the top of the PT. dT/dy will increase with time in-service as the flow bypass in B6S13 develops with increasing diametral creep of the PT. Similarly, $\frac{dC_D}{dy}$ will increase with hot hours as the D concentration profile develops. Therefore, for the flux calculations, the 271279 hot hours of operation were divided into 9 equal intervals with a duration of 301992 HH and the average flux for each interval was determined.

For this assessment, dT/dy is assumed to be linear with hot hours.

The calculation of $\frac{dC_D}{dy}$ for the hot hour intervals is more complicated and was performed along the following steps:

1. Bulk D concentrations at the start and end of each interval were found in Section 4.2.2.1
2. Dissolved D concentrations at the start and the end of each interval were found in Section 4.2.2.2
3. $\frac{dC_D}{dy}$ values at the start and the end of each interval were found as the quotient of the dissolved D concentration and Δy , representing dy .

4.2.2.1 Development of Bulk Deuterium Concentration Profiles with Hot Hours of Operation

Based on the measurements of Table 1, a deuterium concentration of 94 ppm at the side of the PT was attained over 271279 HH of reactor operation at temperature. Under the Bruce Power hypothesis, the D concentration at the side of the developed from D ingress in the RJ, in combination with thermal diffusion, as did the D concentration at the top of the PT of 330 ppm at 271279 HH.

Assuming that the rates of D ingress into the PT at the side and the top of the PT were equal at all times during reactor operation, and that the initial D concentration was 0, the following 2 equations can be written.

$$\Delta C_{D \text{ ingress}} + \Delta C_{D \text{ Diffusion}} = 330 \text{ ppm} \dots\dots 6$$

$$\Delta C_{D \text{ ingress}} - \Delta C_{D \text{ Diffusion}} = 94 \text{ ppm} \dots\dots 7$$

where $\Delta C_{D \text{ ingress}}$ is the concentration of D entering the PT at the BM location due to ingress at the RJ at the side and at the top of the PT, and $\Delta C_{D \text{ Diffusion}}$ is the change in D concentration resulting from thermal diffusion from the side of the PT to the top of the PT.

From Equations 6 and 7, it was predicted that a D concentration of 212 ppm was picked up uniformly around the circumference of the PT at the BM location and that 118 ppm of D had diffused from the side of the PT to the top. For a density of 6440 kg m⁻³ for the hydrided PT material, a concentration of 118 ppm equals 0.76 kg m⁻³. Therefore, it is expected that the top of the PT gained 0.76 kg m⁻³ while the side of the PT lost 0.76 kg m⁻³ over 271279 HH of operation.

For this assessment, it is assumed that the bulk D concentration at the side of the PT and the top of the PT increased linearly with operating time from 0 to 271279 HH.

Figure 7 depicts the bulk D concentration values, in ppm Heq that were determined for the top and the side of the PT at the outlet BM at discrete HH intervals, noting that the corresponding values for dissolved D, discussed later, are also plotted in the figure.

Figure 7
Bulk and Dissolved D Concentrations at the Side and Top of the PT
At the Outlet BM of B6S13 vs HH

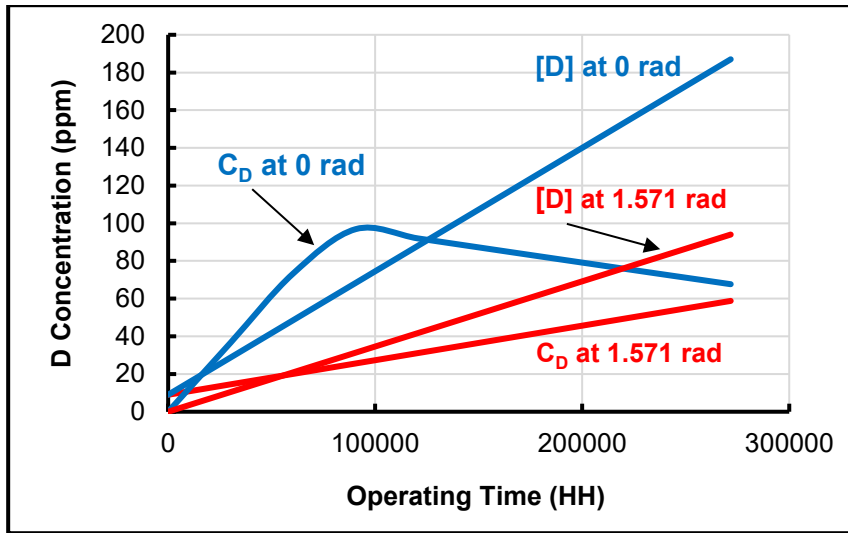
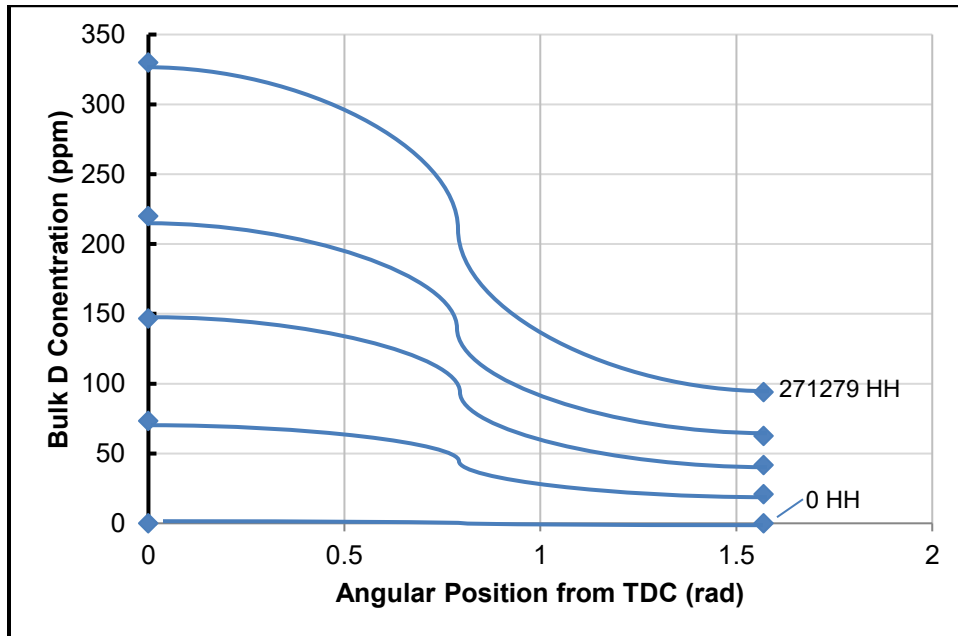


Figure 7 illustrates the development of the bulk D concentration with time at discrete points at the top and the side of the PT at the outlet BM but does not describe the D concentration profile between the top and the side of the PT at the outlet BM.

Figure 8, however depicts the general configuration of the bulk D concentration profiles from 0 to 1.571 rad at the outlet BM as they would have developed over the 271279 HH of operation.

Figure 8
Depiction of Bulk D Concentration vs Angular Position Profiles
at Different Times For the Outlet BM of B6S13



Note that general shape of the profiles represent [D] vs θ adequately, but the shape at the region near the inflection point close to $\theta = 0.8$ rad is inaccurate for each profile.

4.2.2.2 Development of Dissolved Deuterium Concentration Profiles with Hot Hours of Operation

Having determined the bulk D concentrations at the side and the top of the PT at discrete HH values, the next step was to determine the D concentrations in solution with the reactor at hot operating conditions, at discrete HH values.

The following process that was used to predict the dissolved D concentrations is outlined below:

1. The 271729 total HH of operation for B6S13 was divided into 9 intervals containing at total of 10 time steps, each interval with a duration of 30192 HH,
2. The operating temperatures and the bulk Heq concentrations at the top and at the side of the PT were tabulated for each time step,
3. TSSD values at operating temperatures were calculated for the top and the side of the PT for each time step, using Equation 8, below:

$$TSSD = 4.11 \times 10^4 \exp\left(\frac{-28\,000}{RT}\right) \quad [\text{ppm}] \quad \dots\dots\dots 8$$

Where R is universal gas constant and T is the temperature in K.

4. Bulk hydrogen concentrations were tabulated for the top and the side of the PT for each time step, using the H concentration values Table 1 and assuming that the bulk H concentrations were linear with HHs.
5. Next, the dissolved Heq concentrations for the top and the side of the PT at each time step, were determined by comparing the bulk H concentrations to TSSD. The dissolved Heq concentrations were selected as the lesser of TSSD and [Heq].
6. Finally, the dissolved Heq concentrations were converted to dissolved D concentrations, assuming that all the bulk H would have been in solution at each time step.

A summary of the determination of the dissolved D concentrations is given in Table 4.1, the symbols in which are defined in Table 4.2.

Note that the dissolved D concentrations given in Table 4.2 for the side of the PT are considered to be valid for this assessment, as are the dissolved D concentrations at the top of the PT at 0 and at 271279 HH. However, the dissolved D concentrations for the top of the PT, at the intermediate time steps between 0 and 271279 HH are only trial values, since the corresponding [Heq] values were assumed to be linear with HHs, which may not be the case. The treatment of dissolved D concentrations for the top of the PT is detailed further in Section 4.2.2.3.

Table 4.1
Tabulation of Dissolved D Concentrations at the Top and Side of the PT

Time step	HH	T	T	ΔT	TSSD	TSSD	[Heq]		C_H		[H]		C_D	
		1.57 rad	0 rad		1.57 rad	0 rad	1.57 rad	0 rad	1.57 rad	0 rad	1.57 rad	0 rad	1.57 rad	0 rad
	(h)	(°C)			(ppm)									
1	0	308.0	308.0	0.0	64.9	64.9	9.0	9.0	9.0	9.0	9.0	9.0	0.0	0.0
2	30192	308.0	306.7	-1.3	64.9	63.8	14.5	28.8	14.5	28.8	9.3	10.4	10.4	36.7
3	60384	308.0	305.3	-2.7	64.9	62.8	20.1	48.6	20.1	48.6	9.6	11.9	20.9	73.3
4	90576	308.0	304.0	-4.0	64.9	61.8	25.6	68.3	25.6	61.8	9.9	13.3	31.3	96.9
5	120768	308.0	302.7	-5.3	64.9	60.7	31.1	88.1	31.1	60.7	10.2	14.8	41.8	91.9
6	150961	308.0	301.3	-6.7	64.9	59.7	36.7	107.9	36.7	59.7	10.6	16.2	52.2	87.0
7	181153	308.0	300.0	-8.0	64.9	58.7	42.2	127.7	42.2	58.7	10.9	17.7	62.7	82.2
8	211345	308.0	298.7	-9.3	64.9	57.8	47.7	147.4	47.7	57.8	11.2	19.1	73.1	77.3
9	241537	308.0	297.3	-10.7	64.9	56.8	53.3	167.2	53.3	56.8	11.5	20.6	83.6	72.5
10	271729	308.0	296.0	-12.0	64.9	55.8	58.8	187.0	58.8	55.8	11.8	22.0	94.0	67.7

Table 4.2
Definition of Symbols for Table 4.1

HH	Hot hours
T	Operating temperature
ΔT	T difference from the side to the top of the PT
R	Gas constant
TSSD	Terminal Solid Solubility on dissolution in Heq
[H _{eq}]	Bulk hydrogen concentration
C_H	Hydrogen equivalent concentration in solution
H _i	Initial hydrogen concentration
C_D	Deuterium concentration in solution

4.2.2.3 Calculation of Average D Flux over HH Intervals and Total Average D Flux

In this section, the calculations of 4.2.1 for 271279 HH, were repeated for all of the 10 time steps in Table 4.1, in order to determine the average D flux for each 30192 HH interval of operation experienced by B6S13.

The D flux to the top of the PT, presented in Table 3.1 for operation at 271279 h, depends on the temperature and concentration gradients from the side to the top of the PT. $\frac{dT}{dy}$ will increase with

time in-service as the flow bypass in B6S13 develops with increasing diametral creep of the PT.

Similarly, $\frac{dC_D}{dy}$ will increase with hot hours as the D concentration profile develops. Therefore, for the average flux calculations, the 271279 hot hours of operation were divided into 9 equal intervals with a duration of 30192 HH and the average flux for each interval was determined.

For this assessment, $\frac{dT}{dy}$ is assumed to be linear with hot hours.

The calculation of $\frac{dC_D}{dy}$ for the hot hour intervals is more complicated than that for $\frac{dT}{dy}$, as explained below.

At the start and end of each interval, C_D values at the side of the PT are known, but the C_D values at the end of the interval are not known. Therefore, the D flux cannot be calculated directly using Equation 5. However, the C_D value at the top of the OT at the end of each interval depends on the C_D value at the side of the PT and the average flux during the interval. This means that D flux and the C_D value at the top of the PT are interdependent, such that Equation 5 can only be solved by iteration since the final C_D value is not known, which is the case for all the intermediate time steps between 0 and 271279 HH. The first time step at 0 HH and last time step at 271279 HH are exceptions because the C_D values are known and Equation 5 can be solved directly.

The average D flux calculation was performed along the following steps:

1. Bulk D concentrations at the start and end of each interval were found in Section 4.2.2.1
2. Dissolved D concentrations at the start and the end of each interval were found as described in Section 4.2.2.2, noting that trial values of C_D for the top of the PT were used to start the D flux calculations.
3. $\frac{dC_D}{dy}$ values at the start and the end of each interval were found as the quotient of the dissolved D concentration and Δy , representing dy .
4. D flux values at the start and end of each HH interval were calculated using a trial value for C_D at the end of the interval at the top of the PT.
5. The D flux values from Step 4 were used to calculate the resultant C_D at the end of the interval at the top of the PT.
6. For the next iteration to calculate D flux, C_D at the end of the interval at the top of the PT was adjusted to reduce the difference between the trial input value and the calculated value of C_D .
7. The iterations for D flux and C_D at the end of the interval at the top of the PT were repeated until the input and calculated values of C_D at the end of the interval at the top of the PT converged.

A summary of the iterative D flux and C_D calculations is presented in Tables 5.1 – 5.3. Table 5.1 defines the start and end times for the HH intervals and gives the temperatures and dissolved D concentrations at different timesteps during the operation of B6S13 to 271279 HH, as well as the instantaneous D mass flux values at different times.

Table 5.2 provides a summary of the calculations leading to the trial values of average D mass flux for each interval. Table 5.3 presents a summary of the iterative calculations used to generate a final D mass flux value for each interval. Finally, Table 5.3 shows a summary of the final calculation of

the total average D mass flux over 271279 HH of operation and the symbols for Tables 5.1 – 5.3 are defined in Table 5.4.

Some details of the calculations have been omitted from the tables. However, a complete set of detailed calculations for Intervals 1 and 5 are presented as examples in Appendix 1.

Table 5.1
Interval Times, Temperatures, Initial C_{Dn} Values and D Flux due to T Gradient

Interval	t_n	t_{n+1}	T	T	C_{Dn}	C_{Dn}	$J_{\Delta Tn}$
			1.571 rad	0 rad	1.571 rad	0 rad	
	(h)	(h)	(°C)	(°C)	(kg m ⁻³)	(kg m ⁻³)	(kg m ⁻² s ⁻¹)
1	0	30192	308.0	308.0	0.0	0.0	0.00E+00
2	30192.1	60384	308.0	306.7	0.06726	0.06785	1.01E-12
3	60384.2	90576	308.0	305.3	0.13452	0.13713	4.03E-12
4	90576.3	120768	308.0	304.0	0.20179	0.20798	9.06E-12
5	120768.4	150961	308.0	302.7	0.26905	0.28031	1.61E-11
6	150960.6	181153	308.0	301.3	0.33631	0.35418	2.52E-11
7	181152.7	211345	308.0	300.0	0.40357	0.42955	3.62E-11
8	211344.8	241537	308.0	298.7	0.47084	0.50645	4.93E-11
9	241536.9	271729	308.0	297.3	0.5381	0.58486	6.44E-11

Table 5.2
Trial Concentration and D Flux Values for Each Interval

Interval	Trial C_{Dn+1}	Trial C_{Dn+1}	$J_{\Delta Tn+1}$	$J_{\Delta Tav}$	$J_{\Delta Cn}$	$J_{\Delta Cn+1}$	$J_{\Delta Cav}$	$J_{av \text{ int}}$
	1.571 rad	0 rad						
	(kg m ⁻³)	(kg m ⁻³)	(kg m ⁻² s ⁻¹)					
1	0.06726	0.067848	1.01E-12	5.03E-13	0.00E+00	-5.5E-13	-2.7E-13	1.14E-13
2	0.13452	0.137134	4.03E-12	2.52E-12	-5.5E-13	-2.4E-12	-1.5E-12	5.09E-13
3	0.20179	0.207978	9.06E-12	6.54E-12	-2.4E-12	-5.8E-12	-4.1E-12	1.21E-12
4	0.26905	0.280315	1.61E-11	1.26E-11	-5.8E-12	-1.1E-11	-8.2E-12	2.20E-12
5	0.33631	0.354180	2.52E-11	2.06E-11	-1.1E-11	-1.7E-11	-1.4E-11	3.49E-12
6	0.40357	0.429555	3.62E-11	3.07E-11	-1.7E-11	-2.4E-11	-2.1E-11	5.07E-12
7	0.47084	0.506449	4.93E-11	4.28E-11	-2.4E-11	-3.3E-11	-2.9E-11	6.95E-12
8	0.53810	0.584856	6.44E-11	5.69E-11	-3.3E-11	-4.4E-11	-3.9E-11	9.12E-12
9	0.60536	0.664781	8.15E-11	7.30E-11	-4.4E-11	-5.6E-11	-5.0E-11	1.16E-11

Table 5.3
Predicted D Mass Transfer, Final Iteration for D concentration at 0 rad and Total average D Mass Flux

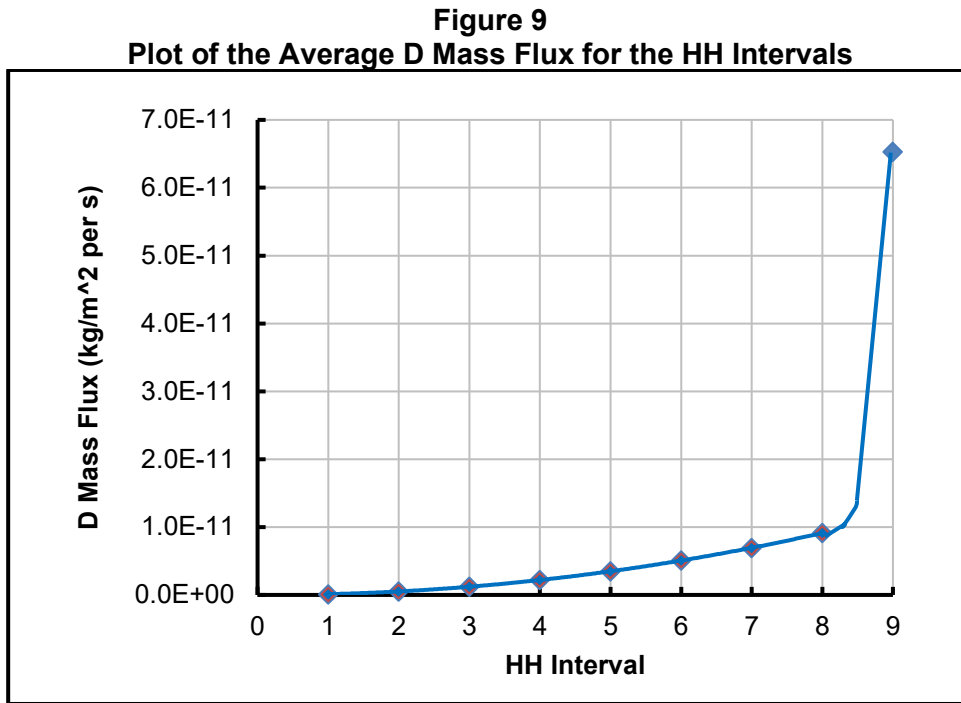
Interval	Δm_D	ΔC_{avD}	C_{Dn+1}	$J_{av \text{ int}}$	$Av J_{av \text{ int}}$
			0 rad		
	(kg)		(kg m ⁻³)	(kg m ⁻² s ⁻¹)	
1	1.2E-11	0.000293	0.067848	1.14E-13	
2	5.5E-11	0.001305	0.137134	5.09E-13	
3	1.3E-10	0.003096	0.207978	1.21E-12	
4	2.4E-10	0.005633	0.280315	2.20E-12	
5	3.8E-10	0.008935	0.354180	3.49E-12	
6	5.5E-10	0.012991	0.429555	5.07E-12	
7	7.6E-10	0.017807	0.506449	6.95E-12	
8	9.9E-10	0.023379	0.584856	9.12E-12	
9	1.3E-09	0.029711	0.664781	6.53E-11	1.044E-11

Note that in Table 5.3, the total average mass flux of D predicted to diffuse into the elemental volume over 271279 HH was entered for the 9th HH interval, and the flux value of 1.044×10^{-11} kg m⁻² s⁻¹ was used in the calculation of Table 6.1.

Table 5.4
Definition of Symbols for Tables 5.1, 5.2, and 5.3

t_n	Time in HH at the start of the nth interval
t_{n+1}	Time in HH at the end of the nth interval
T	Operating temperature
C_{Dn}	D concentration in solution at the start of the nth interval
$J_{\Delta Tn}$	Mass flux of D due to the T gradient at the start of the nth interval
Trial C_{Dn+1}	Trial value for the D concentration in solution at the end of the nth interval
$J_{\Delta Tn+1}$	Mass flux of D due to the T gradient at the end of the nth interval
$J_{\Delta Tav}$	Average mass flux of D due to the T gradient during the interval
$J_{\Delta Cn}$	Mass flux of D due to the C_D gradient at the start of the nth interval
$J_{\Delta Cn+1}$	Mass flux of D due to the C_D gradient at the end of the nth interval
$J_{\Delta Cav}$	Average mass flux of D due to the C_D gradient during the interval
$J_{av \text{ int}}$	Average mass flux of D due to the C_D and T gradients during the interval
Δm_D	Mass of D that diffused into the elemental volume
ΔC_{avD}	Average increase in D concentration in the elemental volume due to diffusion
C_{Dn+1}	D concentration in solution at the end of the nth interval
J_{av}	Average mass flux of D due to the C_D and T gradients for the interval
$Av J_{av \text{ int}}$	Average mass flux of D due to the C_D and T gradients over all intervals to 271279 HH
D_D	Diffusion coefficient for D
Q	Activation energy for H in Zr
R	Universal gas constant
V	Volume in m ³ of the elemental volume
A	Elemental volume cross-sectional area, perpendicular to the circumferential direction
Δt	Duration of the time interval for the diffusion of D

Figure 9 shows the evolution of the average D mass flux to the top of the PT at the outlet BM with operating hours for each 30192 HH interval of operation. The increase in the D mass flux over each HH interval results from the increase in the circumferential temperature gradient as the cold spot at the top of the PT develops with increasing flow bypass, with time in-service.



4.2.2.4 Prediction of the Mass of Deuterium that would have Migrated from the Side to the Top of the PT by Thermal Diffusion

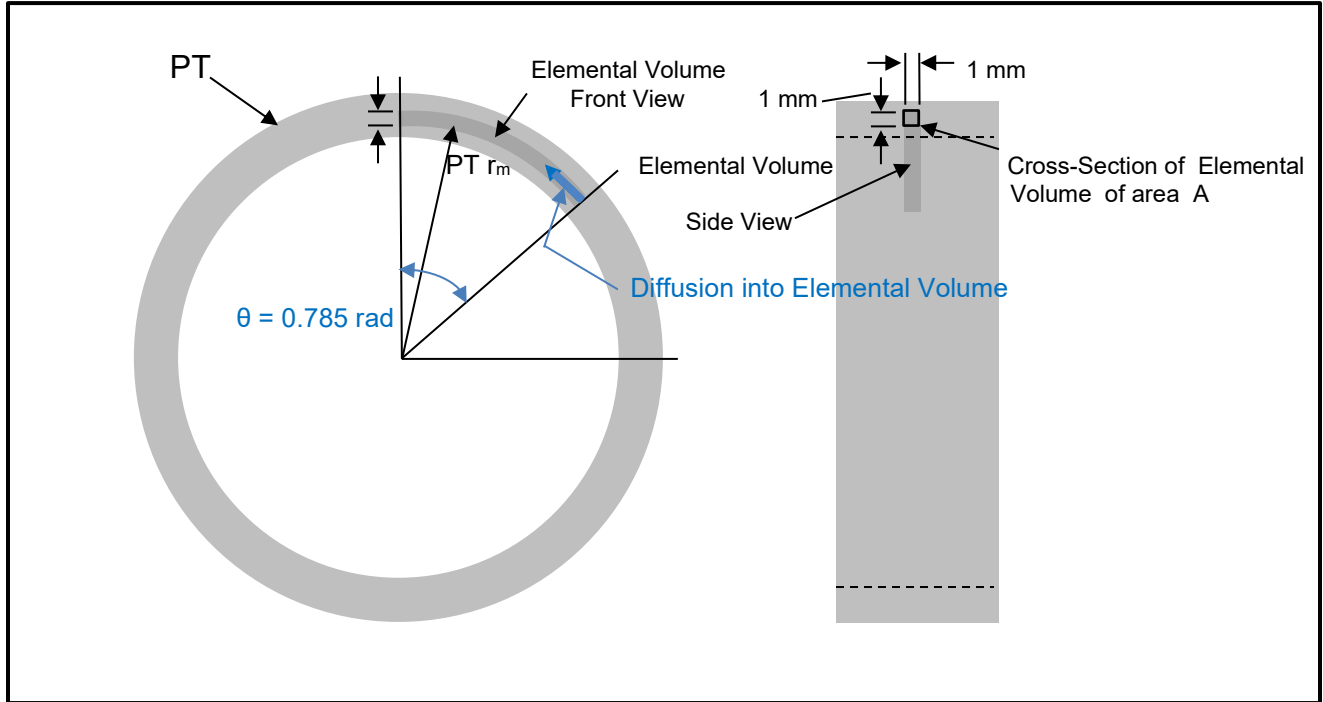
Knowing the total average D flux from the side of the PT to the top of the PT from Section 4.2.2.3 over 271279 HH of operation, the corresponding amount of D that would have diffused to the top of the PT can readily be calculated. Specifically, for a given mass flux, the mass of deuterium that would have diffused from an elemental volume at the side of the PT to a similar elemental volume at the top of the PT over 271279 HH can be calculated using:

$$\Delta m_D = J_{total} \bullet A \bullet \Delta t \dots\dots\dots 9$$

where Δm_D is the mass of D that diffused over 271279 HH
 J_{total} is the total average D mass flux from 0 to 271279 HH
 A is the cross-sectional area of the elemental volume, perpendicular to the diffusion flux, through which the D entered the volume at the top of the PT

Figure 10 illustrates the elemental volume for the D mass calculation of Equation 9. The elemental volume is a circular arch with a square cross-section. The radius of the centroid of the cross-section of the arch is the same as the mean radius of the PT, with a nominal dimension of 54.04 mm. The cross-sectional dimensions of the area A, were chosen to be 1 mm x 1 mm. As shown in the figure, the elemental volume starts at the cross-section at $\theta = 0.785$ rad and ends at the cross-section at $\theta = 0$ rad. The D that diffused into the elemental volume entered the volume with an average D mass flux of 1.044×10^{-11} kg m⁻² s⁻¹ through the cross-sectional area A.

Figure 10
Illustration of the Elemental Volume for the Diffusion of D to the Top of the PT



The D mass calculation is summarised in Table 6.1. The symbols for Table 6.1 are defined in Table 6.2.

Table 6.1
Summary of the Calculation of the Mass of D Diffused into the Elemental Volume

J_{total}	t_0	t_f	Δt	Δt	A	Δm_D
$(\text{kg m}^{-2} \text{ s}^{-1})$	(HH)	(HH)	(HH)	(s)	(m^2)	(kg)
1.044E-11	0	271729	271729	9.8E+08	1.00E-06	2.043E-08

Table 6.2
Definition of Symbols for Table 6.1

J_{total}	Average mass flux of D due to the C_D and T gradients over all intervals to 271279 HH
t_0	Time in HH at the start of the D diffusion process
t_f	Time in HH at the en of the D diffusion process
Δt	Duration in HH of the D diffusion process
A	Elemental volume cross-sectional area, perpendicular to the circumferential direction
Δm_D	Mass of D diffused into the elemental volume over 271279 HH

From Table 6.1, the predicted mass of D that would have diffused into the elemental volume at the outlet BM due to thermal diffusion over 217279 HH is 2.043×10^{-8} kg.

4.2.3 Estimation of the Mass of Deuterium that Diffused from the Side to the Top of the PT at the BM Based on D Concentration Measurements

In Section 4.2.2.1, it was determined that a D concentration of 212 ppm was picked up uniformly around the circumference of the PT at the BM location and that 118 ppm of D had diffused from the side of the PT to the top. For a density of 6440 kg m^{-3} for the hydrided PT material, a concentration of 118 ppm equals 0.76 kg m^{-3} . Therefore, it is expected that the local point at the top of the PT gained 0.76 kg m^{-3} while the local point at the side of the PT lost 0.76 kg m^{-3} over 271279 HH of operation due to thermal diffusion.

From this result, the mass of deuterium that would have diffused from one side of the PT to the top of the PT, by thermal diffusion was calculated, as follows:

1. For the D concentration data above, a circumferential D concentration distribution was generated by fitting a cosine function to concentration $[D_{\text{dif}}]$ versus angular position, θ as depicted in Figure 11. $[D_{\text{dif}}]$ is the bulk concentration of D established by diffusion.
2. The cosine function was integrated with respect to θ to find the area under the curve, representing the product of $[D_{\text{dif}}] \times \theta$ from 0 to 0.7854 rad, which is the region into which the diffusion occurred.
3. The integrand $[D_{\text{dif}}] \theta$ from 0 to 0.7854 rad was divided by θ to obtain the average D concentration, $D_{\text{dif}}]_{\text{av}}$ in the region from 0 to 0.7854 rad.
4. To determine the mass of D that had diffused into the region from 0 to 0.7854 rad, an elemental volume was defined. The volume consists of a circular arc with a mean radius of 54 mm, the same as that of the PT, with a square cross-section, arbitrarily measuring 1 mmx1 mm. The elemental volume ranges from 0 to 0.785 radians.
5. Then the mass of D inside the elemental volume was found as the product of $[D_{\text{dif}}]_{\text{av}}$ and V.

A summary of calculations for Steps 1 – 5 is presented in Table 7.1, below and the nomenclature for Table 7.1 is explained in Table 7.2.

Figure 11
Concentration of Diffused D in the B6S13 Outlet BM at 271k HH
Versus Angular Position

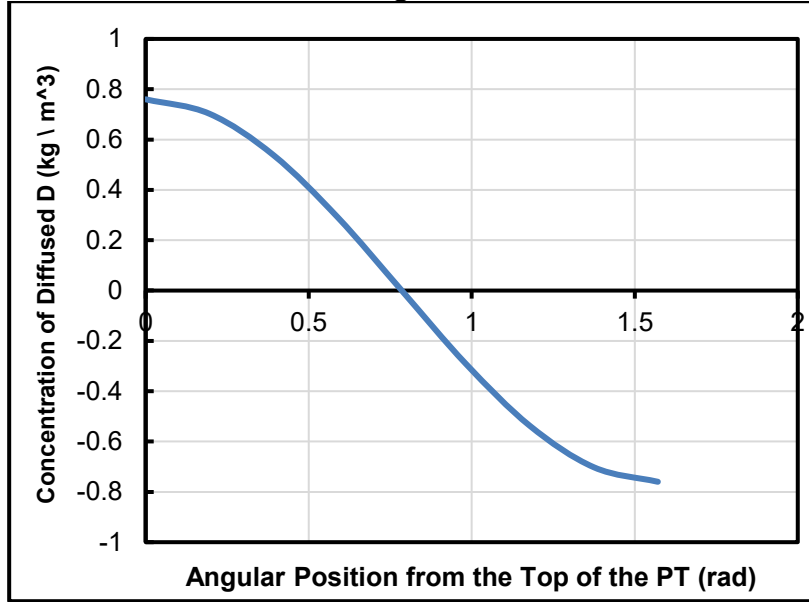


Table 7.1
Calculation of the Mass of D that Diffused from the Side to the Top of the PT

x	θ	[D]	ρ_{PT}	[D _{dif}]	$\Delta[D_{dif}]$	PT r_m	Δy	V	Calculate [D _{dif}] _{av}			Δm_D
									θ	$\int [D_{dif}] d\theta$	[D _{dif}] _{av}	
(mm)	(rad)	(ppm)		(kg m ⁻³)		(m)	(m)	(m ⁻³)	(rad)	(kg m ⁻³ rad)	(kg m ⁻³)	(kg)
69	0	330	6440	2.125	0.760	0.054	0.085	4.2E-08	0.785	0.380	0.484	2.054E-08
69	1.571	94	6440	0.605	-0.760							

Table 7.2
Definition of Symbols for Table 7.1

x	Axial distance from the PT outlet end
θ	Angular position from Top Dead Centre
[D _{dif}]	Bulk D concentration due to diffusion
ρ_{PT}	Density of PT material including H and D content
$\Delta[D_{dif}]$	D concentration increment from circumferential thermal diffusion at the BM
PT r_m	Mean radius of the PT
Δy	Arclength of the elemental volume for diffusion analysis
V	Volume of the elemental volume for diffusion analysis
[D _{dif}] _{av}	Average concentration of the D that diffused into the elemental volume
Δm_D	Mass of D that diffused into the elemental volume over 271729 HH

In the table, the bulk D concentration, [D] was converted from ppm to kg m⁻³, assuming a density of 6440 kg m⁻³ for the hydride PT material. $\Delta[D_{dif}]$ represents the increase in concentration in the concentration profile from $\theta = 1.571$ rad to $\theta = 0$ rad that was due to thermal diffusion alone. V represents an elemental volume of PT material sweeping out an arc of 45 degrees from $\theta = 0$ rad to

$\theta = 0.785$ rad that would have undergone a distributed bulk D concentration increase, $\Delta[D_{dif}]$ ranging from 0.760 kg m^{-3} at $\theta = 0$ rad to 0 kg m^{-3} at $\theta = 0.785$ rad over 271729 hot hours.

As indicated in Table 7.1, it was calculated that a total mass of $2.054 \times 10^{-8} \text{ kg}$ of D, distributed within the elemental volume of $4.2 \times 10^{-8} \text{ m}^3$ would be consistent with the concentration profile of Figure 11. In other words, the bulk D concentration measurements for the outlet BM of B6S13 indicate that $2.054 \times 10^{-8} \text{ kg}$ of D had actually diffused into the elemental volume over 271729 HH of operation.

5. Discussion of Results

In Section 4.2.3, bulk D concentration measurements were used to calculate that the observed circumferential D profile at the outlet BM of B6S13 meant that $2.054 \times 10^{-8} \text{ kg}$ of D had actually diffused into the elemental volume over 271729 HH of operation.

In Section 4.4.2, an independent theoretical calculation of the average mass flux of D from the side of the PT to the top of the PT, using an assumed temperature distribution, was performed to predict the mass of D that would have diffused into the same elemental volume by thermal diffusion over 271279 HH. As indicated in Section 4.2.2, it was predicted that thermal diffusion would have driven $2.043 \times 10^{-8} \text{ kg}$ of D into the elemental volume over 271279 HH.

Therefore, the theoretical prediction of the diffusion of $2.043 \times 10^{-8} \text{ kg}$ of D into the elemental volume over 271279 HH agrees very closely with the empirically-based calculation of $2.054 \times 10^{-8} \text{ kg}$ as the mass of D that had diffused into the elemental volume over 271279 HH.

The accuracy of the predicted mass of D that diffused into the elemental volume is somewhat surprising given that the actual diffusion of D in the B6S13 outlet RJ is more complex than the simple 1-dimensional expression of Equation 5.

Regardless, the results of this analysis support the Bruce Power Hypothesis that thermal diffusion caused the D concentration gradients observed in the outlet RJ of B6S13.

Although the high circumferential [D] gradient in the outlet of B6F13 did cause concerns about the modelling of D ingress in the RJ and will affect the fracture toughness at the top of the PT, the diffusion of H/D to the top of the PT, where flaws are not expected, will reduce the Heq concentration in the lower regions of the PT, where flaw generation is possible. The diffusion of H/D to the top of the PT in B6S13, where no flaws are expected, would delay the onset of hydride ratchetting at potential flaws near the bottom of the PT which would theoretically benefit the PT, provided that no dispositionable flaws are present in the top region of the PT where the Heq concentration is elevated.

6. Conclusions

1. For the operating temperature distribution specified below, the measured circumferential [D] gradient at the outlet BM of B6S13 is entirely attributable to thermal diffusion over a period of 217279 HH, in agreement with the Bruce Power hypothesis.

The operating temperature profile at the outlet BM of B6S13 assumed for this assessment is as follows:

- At 0 HH, the operating temperatures at the top and side of the PT at the outlet BM equalled 308 °C.
 - At 271279 HH, the operating temperature at the top of the PT at the outlet BM remained at 308 °C, and the side of the PT at the outlet BM operated at 296 °C.
 - At all intermediate HH values, the operating temperature at the top of the PT at the outlet BM remained at 308 °C and the operating temperature at the side at the outlet BM varied linearly with HH of operation from 308 °C to 296 °C.
2. It was postulated in Reference [1] that electrochemical diffusion from a strong point source in the outlet RJ could have contributed to the [D] concentration gradient seen in B6S13. From Conclusion 1, there is no longer a rationale for postulating the existence of a novel point source of D at the top of the RJ in B6S13 as thermal diffusion is a sufficient explanation.

7. References

1. Review of Bruce Power Submissions on Elevated Heq in Pressure Tube Rolled Joints and Independent Analysis of Possible Causes, Technical Report to the CNSC for the Public Hearing on Elevated Heq Measurements in the Bruce NGS Pressure Tubes, P. Sedran, RESD Inc., October 15, 2022.
2. .CNSC CMD 23-M27 Mid-Term Report Presentation, Bruce Power Mid-Term Update of Licensed Activities, June 8, 2023.
3. CMD 23-M27.1 Bruce Power Mid-Term Update of Licensed Activities, Written Submission from Bruce Power, File 6.02.04, June 6, 2023.

8. Appendix 1- Detailed Summary Table for Diffusion Calculations

Appendix 1 provides a detailed summary of the iterative calculations of D mass flux for HH intervals 1 and 5. The same diffusion flux calculations were performed for all 9 HH intervals, of duration 30192 HH. The objective of the calculations for each interval was to predict the average D mass flux for the interval. For each interval, iteration was performed by changing the final CD value at 0 radians until the trial value converged to the calculated value of CD. As an example, for interval 5, it can be seen how Trial C_{Dn+1} at 0 rad in Table A1-3.2 converges to C_{Dn+1} at 0 rad in Table A1-3.4

Table A1-1
Physical Constants that are the Same in Each Iteration of Equation 5

T	Δy	D_D	Q	R	V	A
1.571 rad		1.571 rad				
(°C)	(m)	(m ² s ⁻¹)	(J/mol)	(JK ⁻¹ mol ⁻¹)		
308.0	0.085	7.96E-11	33600	8.313	4.2E-08	1E-06

Table A1-2.1
Columns 1 – 11 of Calculation Table for HH Interval 1

Interval/ Iteration	t_n	t_{n+1}	T	ΔT_n	ΔT_{n+1}	$\Delta T/\Delta y_n$	C_{Dn}			$J_{\Delta Tn}$
			0 rad				1.571 rad		0 rad	
	(h)	(h)	(°C)	(°C)	(°C)	(°C/m)	(ppm)	(kg m ⁻³)	(kg m ⁻³)	(kg m ⁻² s ⁻¹)
1/1	0	30192	308.0	0.00	-1.33	0.0	0.0	0.0	0.0	0.0
1/2	0	30192	308.0	0.00	-1.33	0.0	0.0	0.0	0.0	0.0
1/3	0	30192	308.0	0.00	-1.33	0.0	0.0	0.0	0.0	0.0
1/4	0	30192	308.0	0.00	-1.33	0.0	0.0	0.0	0.0	0.0
1/5	0	30192	308.0	0.00	-1.33	0.0	0.0	0.0	0.0	0.0
1/6	0	30192	308.0	0.00	-1.33	0.0	0.0	0.0	0.0	0.0
1/7	0	30192	308.0	0.00	-1.33	0.0	0.0	0.0	0.0	0.0
1/8	0	30192	308.0	0.00	-1.33	0.0	0.0	0.0	0.0	0.0

Table A1-2.2
Columns 1 and 12 – 17 of Calculation Table for HH Interval 1

Interval/ Iteration	$\Delta T/\Delta y_{n+1}$	Trial C_{Dn+1}			$J_{\Delta Tn+1}$	$J_{\Delta Tav}$
		1.571 rad	1.571 rad	0 rad		
	(°C/m)	(ppm)	(kg m ⁻³)	(kg m ⁻³)	(kg m ⁻² s ⁻¹)	
1/1	-15.7	10.4	0.06726	0.06701000	1.01E-12	5.03E-13
1/2	-15.7	10.4	0.06726	0.06793256	1.01E-12	5.03E-13
1/3	-15.7	10.4	0.06726	0.06783951	1.01E-12	5.03E-13
1/4	-15.7	10.4	0.06726	0.06784889	1.01E-12	5.03E-13
1/5	-15.7	10.4	0.06726	0.06784795	1.01E-12	5.03E-13
1/6	-15.7	10.4	0.06726	0.06784804	1.01E-12	5.03E-13
1/7	-15.7	10.4	0.06726	0.06784803	1.01E-12	5.03E-13
1/8	-15.7	10.4	0.06726	0.06784803	1.01E-12	5.03E-13

Table A1-2.3
Columns 1 and 13 – 19 of Calculation Table for HH Interval 1

Interval/ Iteration	$\Delta C_D/\Delta y_n$	$\Delta C_D/\Delta y_{n+1}$	$J_{\Delta Cn}$	$J_{\Delta Cn+1}$	$J_{\Delta Cav}$	$J_{av int}$
	(kg m ⁻⁴)	(kg m ⁻⁴)	(kg m ⁻² s ⁻¹)			
	0.000	-0.002973	0.00E+00	2.4E-13	1.2E-13	3.1E-13
1/1	0.000	0.007902	0.00E+00	-6.3E-13	-3.1E-13	9.4E-14
1/2	0.000	0.006805	0.00E+00	-5.4E-13	-2.7E-13	1.2E-13
1/3	0.000	0.006916	0.00E+00	-5.5E-13	-2.8E-13	1.1E-13
1/4	0.000	0.006904	0.00E+00	-5.5E-13	-2.7E-13	1.1E-13
1/5	0.000	0.006905	0.00E+00	-5.5E-13	-2.7E-13	1.1E-13
1/6	0.000	0.006905	0.00E+00	-5.5E-13	-2.7E-13	1.1E-13
1/7	0.000	0.006905	0.00E+00	-5.5E-13	-2.7E-13	1.1E-13
1/8	0.000	0.006905	0.00E+00	-5.5E-13	-2.7E-13	1.1E-13

Table A1-2.4
Columns 1 and 20 – 26 of Calculation Table for HH Interval 1

Interval/ Iteration	Δt	Δm_D	ΔC_{avD}	C_{Dn+1}	C_{Dn+1}	J_{av}
				0 rad	0 rad	
	(s)	(kg)	(kg m ⁻³)	(ppm)	(kg m ⁻² s ⁻¹)	
1/1	1.1E+08	3.4E-11	8.0E-04	0.06885513		
1/2	1.1E+08	1.0E-11	2.4E-04	0.06774645		
1/3	1.1E+08	1.3E-11	3.0E-04	0.06785828		
1/4	1.1E+08	1.2E-11	2.9E-04	0.06784700		
1/5	1.1E+08	1.2E-11	2.9E-04	0.06784814		
1/6	1.1E+08	1.2E-11	2.9E-04	0.06784802		
1/7	1.1E+08	1.2E-11	2.9E-04	0.06784804		
1/8	1.1E+08	1.2E-11	2.9E-04	0.06784803	10.535	1.143E-13

Table A1-3.1
Columns 1 – 11 of Calculation Table for HH Interval 5

Interval/ Iteration	t_n	t_{n+1}	T	ΔT_n	ΔT_{n+1}	$\Delta T/\Delta y_n$	C_{Dn}			$J_{\Delta Tn}$
			0 rad				1.571 rad	1.571 rad	0 rad	
			(h)				(h)	(°C)	(°C)	
5/1	120768	150961	302.7	-5.33	-6.67	-62.87	41.78	0.27	0.28	1.61E-11
5/2	120768	150961	302.7	-5.33	-6.67	-62.87	41.78	0.27	0.28	1.61E-11
5/3	120768	150961	302.7	-5.33	-6.67	-62.87	41.78	0.27	0.28	1.61E-11
5/4	120768	150961	302.7	-5.33	-6.67	-62.87	41.78	0.27	0.28	1.61E-11
5/5	120768	150961	302.7	-5.33	-6.67	-62.87	41.78	0.27	0.28	1.61E-11
5/6	120768	150961	302.7	-5.33	-6.67	-62.87	41.78	0.27	0.28	1.61E-11
5/7	120768	150961	302.7	-5.33	-6.67	-62.87	41.78	0.27	0.28	1.61E-11
5/8	120768	150961	302.7	-5.33	-6.67	-62.87	41.78	0.27	0.28	1.61E-11
5/9	120768	150961	302.7	-5.33	-6.67	-62.87	41.78	0.27	0.28	1.61E-11
5/10	120768	150961	302.7	-5.33	-6.67	-62.87	41.78	0.27	0.28	1.61E-11
5/11	120768	150961	302.7	-5.33	-6.67	-62.87	41.78	0.27	0.28	1.61E-11
5/12	120768	150961	302.7	-5.33	-6.67	-62.87	41.78	0.27	0.28	1.61E-11

Table A1-3.2
Columns 1 and 12 – 17 of Calculation Table for HH Interval 5

Interval/ Iteration	$\Delta T/\Delta y_{n+1}$	Trial C_{Dn+1}			$J_{\Delta T_{n+1}}$	$J_{\Delta T_{av}}$
		1.571 rad	1.571 rad	0 rad		
	(°C/m)	(ppm)	(kg m ⁻³)	(kg m ⁻³)	(kg m ⁻² s ⁻¹)	
5/1	-78.58484	52.2	0.3363111	0.0670100	2.52E-11	2.06E-11
5/2	-78.58484	52.2	0.3363111	0.3831461	2.52E-11	2.06E-11
5/3	-78.58484	52.2	0.3363111	0.3512586	2.52E-11	2.06E-11
5/4	-78.58484	52.2	0.3363111	0.3544750	2.52E-11	2.06E-11
5/5	-78.58484	52.2	0.3363111	0.3541506	2.52E-11	2.06E-11
5/6	-78.58484	52.2	0.3363111	0.3541833	2.52E-11	2.06E-11
5/7	-78.58484	52.2	0.3363111	0.3541800	2.52E-11	2.06E-11
5/8	-78.58484	52.2	0.3363111	0.3541803	2.52E-11	2.06E-11
5/9	-78.58484	52.2	0.3363111	0.3541803	2.52E-11	2.06E-11
5/10	-78.58484	52.2	0.3363111	0.3541803	2.52E-11	2.06E-11
5/11	-78.58484	52.2	0.3363111	0.3541803	2.52E-11	2.06E-11
5/12	-78.58484	52.2	0.3363111	0.3541803	2.52E-11	2.06E-11

Table A1-3.3
Columns 1 and 13 – 19 of Calculation Table for HH Interval 5

Interval/ Iteration	$\Delta C_D/\Delta y_n$	$\Delta C_D/\Delta y_{n+1}$	$J_{\Delta C_n}$	$J_{\Delta C_{n+1}}$	$J_{\Delta C_{av}}$	$J_{av \text{ int}}$
	(kg m ⁻⁴)	(kg m ⁻⁴)	(kg m ⁻² s ⁻¹)			
	0.1328003	-3.17445	-1.06E-11	2.53E-10	1.21E-10	7.08E-11
5/1	0.1328003	0.552078	-1.06E-11	-4.39E-11	-2.72E-11	-3.31E-12
5/2	0.1328003	0.176197	-1.06E-11	-1.40E-11	-1.23E-11	4.17E-12
5/3	0.1328003	0.214111	-1.06E-11	-1.70E-11	-1.38E-11	3.42E-12
5/4	0.1328003	0.210287	-1.06E-11	-1.67E-11	-1.36E-11	3.49E-12
5/5	0.1328003	0.210672	-1.06E-11	-1.68E-11	-1.37E-11	3.49E-12
5/6	0.1328003	0.210633	-1.06E-11	-1.68E-11	-1.37E-11	3.49E-12
5/7	0.1328003	0.210637	-1.06E-11	-1.68E-11	-1.37E-11	3.49E-12
5/8	0.1328003	0.210637	-1.06E-11	-1.68E-11	-1.37E-11	3.49E-12
5/9	0.1328003	0.210637	-1.06E-11	-1.68E-11	-1.37E-11	3.49E-12
5/10	0.1328003	0.210637	-1.06E-11	-1.68E-11	-1.37E-11	3.49E-12
5/11	0.1328003	0.210637	-1.06E-11	-1.68E-11	-1.37E-11	3.49E-12

Table A1-3.4
Columns 1 and 20 – 26 of Calculation Table for HH Interval 5

Interval/ Iteration	Δt	Δm_D	ΔC_{avD}	C_{Dn+1}	C_{Dn+1}	J_{av}
				0 rad	0 rad	
	(s)	(kg)	(kg m ⁻³)		(ppm)	(kg m ⁻² s ⁻¹)
5/1	1.1E+08	7.7E-09	1.8E-01	0.6992822		
5/2	1.1E+08	-3.6E-10	-8.5E-03	0.3193711		
5/3	1.1E+08	4.5E-10	1.1E-02	0.3576914		
5/4	1.1E+08	3.7E-10	8.8E-03	0.3538261		
5/5	1.1E+08	3.8E-10	9.0E-03	0.3542160		
5/6	1.1E+08	3.8E-10	8.9E-03	0.3541767		
5/7	1.1E+08	3.8E-10	8.9E-03	0.3541807		
5/8	1.1E+08	3.8E-10	8.9E-03	0.3541803		
5/9	1.1E+08	3.8E-10	8.9E-03	0.3541803		
5/10	1.1E+08	3.8E-10	8.9E-03	0.3541803		
5/11	1.1E+08	3.8E-10	8.9E-03	0.3541803		
5/12	1.1E+08	3.8E-10	8.9E-03	0.3541803	54.99693985	3.487E-12

Definition of Symbols

t_n	Time in HH at the start of the nth interval
t_{n+1}	Time in HH at the end of the nth interval
T	Operating temperature
C_{Dn}	D concentration in solution at the start of the nth interval
$J_{\Delta Tn}$	Mass flux of D due to the T gradient at the start of the nth interval
Trial C_{Dn+1}	Trial value for the D concentration in solution at the end of the nth interval
$J_{\Delta Tn+1}$	Mass flux of D due to the T gradient at the end of the nth interval
$J_{\Delta T_{av}}$	Average mass flux of D due to the T gradient during the interval
$J_{\Delta Cn}$	Mass flux of D due to the C_D gradient at the start of the nth interval
$J_{\Delta Cn+1}$	Mass flux of D due to the C_D gradient at the end of the nth interval
$J_{\Delta C_{av}}$	Average mass flux of D due to the C_D gradient during the interval
$J_{av \text{ int}}$	Average mass flux of D due to the C_D and T gradients during the interval
Δm_D	Mass of D that diffused into the elemental volume
ΔC_{avD}	Average increase in D concentration in the elemental volume due to diffusion
C_{Dn+1}	Concentration of D in solution at the end of the interval
J_{av}	Average mass flux of D for the interval
Av $J_{av \text{ int}}$	Average mass flux of D over all the intervals, from 0 to 271279 HH
D_D	D diffusion coefficient
Q	Activation energy of diffusion
R	Gas Constant
V	Volume of the elemental volume
A	Cross-sectional area fro diffusion into the elemental volume
Δt	Duration of the time interval

9. Appendix 2 - Review of References [1] and [2]

9.1 Review of CNSC Document, Reference [1]

The document in question is the CNSC Staff Presentation CMD 23-M27, Bruce Power Mid-term Update of Licensed Activities. The review was limited to the topic of elevated Heq concentrations in the pressure tubes.

The following are comments from the review.

1. General Terminology

Bruce Power has contended that the elevated Heq concentrations at the top of the PTs are due to a redistribution of H/D, which has been independently confirmed by the diffusion analysis of Section 4. Elevated Heq concentrations imply a general and overall significant increase in Heq concentrations but this is not the case in B6S13. The situation in B6S13 would be more accurately described as a redistribution of H/D to the top of the PT (considered to be free of flaws) from the lower regions of the PT where in-service flaw generation is possible. It is proposed that future documents from the CNSC would benefit from a change in terminology from “elevated Heq concentrations” to the “circumferential redistribution of Heq concentrations.”

2. Validity of the RJ D Ingress Model

Previously, the CNSC had stated that the D concentration measurements in B6S13 were inconsistent with the current industry model for RJ D ingress. The concern was that the existing model was inadequate for assessing the PTs and the implication was that further theoretical development of the RJ D ingress model would be necessary to ensure the accuracy of PT integrity assessments. However, there was no mention of the issue of the validity of the RJ D ingress model in the CNSC Staff Presentation. A reader of the previous documents on the subject would notice the absence of any discussion of that issue in the CNSC Staff Presentation. For this reason, it is proposed that the CNSC Staff Presentation should address the validity of the current RJ D ingress model in order to follow up and bring resolution to the CNSC’s previous comments. The following text is proposed:

The current RJ D ingress model considers only axial diffusion of H/D in the RJ region and so, is one dimensional. Therefore, there is no prediction of circumferential diffusion in the model, but the axial diffusion equations in the model could readily be applied to the circumferential direction to predict axial and circumferential diffusion, as observed in B6S13. Two-dimensional diffusion analysis capability exists in BP’s H3DMap code and was used to simulate the diffusion process observed in B6S13. Overall, the failure of the RJ D ingress to predict circumferential diffusion does not indicate a serious theoretical misunderstanding or technical flaw in the model. Instead, it was discovered that the assumption of one-dimensional axial diffusion, which was reasonable at the time, and applies early in the life of all PTs, was not valid later in the operating life of B6S13 because of the thermal gradient resulting from flow bypass.

9.2 Review of Bruce Power Submission, Reference [2]

The document in question is the Bruce Power Submission, CMD 23-M27-1, Bruce Power Mid-term Update of Licensed Activities. The review was limited to the topic of elevated Heq concentrations in the pressure tubes.

The following are comments from the review.

1. The lead paragraph highlights BP's commitment to safety and then mentions transparency about a technical issue. The paragraph could result in the association of the technical issue with nuclear safety issues. This is unnecessary and is technically incorrect. The following wording is proposed:

Bruce Power remains committed to openness and transparency with both the public and Canadian Nuclear Safety Commission (CNSC) regarding a non-safety technical issue that it had proactively disclosed to the CNSC in 2021.

2. In the second paragraph, the technical issue is described as higher than anticipated hydrogen concentration readings. Considering what is currently known about the elevated Heq concentration measurements, the statement is quite uninformative. Presently, the situation is much better understood, such the elevated Heq concentration measurements could be described as a circumferential redistribution of H/D. The following wording is proposed:

As part of Bruce Power's ongoing planned inspection, testing, analysis and maintenance activities, some higher than anticipated hydrogen equivalent concentration readings were observed in two units, both of which were not operating at the time. The elevated readings were attributed to the circumferential redistribution of hydrogen in the PT due to thermal diffusion to a cold spot at the top of the PT, associated with flow bypass in the PT.

Further, from the perspective of PT fitness-for-service, the diffusion of H/D from the bottom of the PT, where in-service flaws could be generated, to the top of the PT, where any flaws are highly unlikely, could be of benefit to the PT. The circumferential redistribution of H/D would delay the onset of hydride ratchetting at potential flaws at the bottom of the PT, providing some benefit to the PT. Bruce Power could emphasize that (1) the circumferential thermal diffusion of H/D is well understood theoretically and can be accurately predicted using standard diffusion equations, (2) the diffusion of H/D to the top of the PT means that H/D was removed from the bottom of the PT. Theoretically, provided that there are no flaws near the top of the PT, margins on PT fitness-for-service could be higher with circumferential diffusion than without it.

3. The third paragraph refers to the hydrogen levels being the Bruce Power operating license. The exact meaning of the statement is not clear. Is the intended meaning that the Heq concentration levels are within the limits (120 ppm) which is specified in the operating license. The complication here is that B6S13 exceeds 120 ppm at the outlet BM. As such, the text of the third paragraph needs some clarification.
4. There is considerable concern from the CNSC about the exceedance of the 120 ppp Heq concentration, as exemplified in B6S13. Since the limit on H/D concentration is related to fracture toughness considerations, it may be possible for Bruce Power to derive a concentration limit for PT material that could be susceptible to flaws and a higher limit for

regions of the PT that are free of flaws. In this way, PTs like B6S13, that currently exceed the 120 ppm limit at the top of the PT, would not exceed the maximum allowable Heq concentration.

5. The diffusion code RJDIM will have to be modified to account for 2-dimensional diffusion for future assessments, or H3DMAP will have to be used. Will Bruce Power be performing reanalyses for the existing RJ [D] predictions produced with RJDIM?